Seventh International Conference on Computational Fluid Dynamics (ICCFD7), Big Island, Hawaii, July 9-13, 2012

ICCFD7-3704

Application of a K-ϵ Turbulence Model to Reshocked Richtmyer–Meshkov Instability Corresponding to a Heavy-to-Light Gas Transition

J. Tiberius Morán-López*, James P. Holloway* and Oleg Schilling**
Corresponding author: schilling1@llnl.gov
*Department of Nuclear Engineering and Radiological Sciences
Center for Radiative Shock Hydrodynamics (CRASH)
University of Michigan, Ann Arbor MI 48109, USA.
**Lawrence Livermore National Laboratory, Livermore CA 94550, USA.

Abstract: Reshocked Richtmyer–Meshkov turbulent mixing of sulfur hexafluoride (SF_6) and air for Atwood number $At = -0.67$ and incident shock Mach number $Ma_s = 1.45$ is simulated using a third-order weighted essentially nonoscillatory (WENO) finite-difference implementation of a two-equation K-ϵ multicomponent Reynolds-averaged Navier–Stokes (RANS) model. Experimental measurements [F. Poggi et al., Physics of Fluids 10 (1998), 2698] and previous numerical results using the BHR turbulence model [A. Banerjee et al., Phys. Rev. E 82 (2010) 046309] for the mixing layer width before and after reshock, along with analytical self-similar power-law solutions of the simplified model equations before reshock, are compared with the evolution of the predicted mixing layer widths. Sensitivity to variations in the turbulent kinetic energy seed, initial perturbation wavelength, and incident shock Mach number were investigated. Smaller shock Mach numbers led to later reshock times, decrease in initial growth, and other effects in post-reshock mixing depending on the two key model coefficients. Changes in the shock production model coefficients, $C_{\epsilon 0}$ and σ_ρ, affected the predicted mixing layer widths after reshock, but had minimal effect on the growth prior to reshock.

Keywords: Turbulence Modeling, Multicomponent Reynolds-Averaged Navier–Stokes, Richtmyer–Meshkov Instability, Reshock.

1 Introduction

Understanding the effects of turbulence generated by multifluid hydrodynamic instabilities is of critical importance to many applications in science and engineering. Of particular interest is the study of turbulence effects in high-energy-density and astrophysical environments [1] such as supernovae, inertial confinement fusion (ICF) capsule implosions, and shock tube flows. Related examples include high-energy-density laser experiments and the mixing of gases in stellar interiors. Blast waves and shock instabilities [2] are critical to the formation of supernovae and also have important roles in stellar and galaxy formation.

Turbulent mixing via reshocked Richtmyer–Meshkov instability is one important mechanism through which turbulence is generated by the interactions of shock waves with material interfaces in fluids. For example, in supernovae and ICF capsule implosions, turbulent mixing originating from this instability is generated as shocks traverse perturbed interfaces separating fluids of different densities; shocks impulsively accelerate the interfaces and induce perturbation growth and eventually turbulent mixing at sufficiently large Reynolds numbers. The shock can be generated in either the light or the heavy fluid to impulsively accelerate the first fluid towards the second. In many applications the evolving interface and resulting mixing layer are *reshocked* by a reflected shock. Such reshocked Richtmyer–Meshkov instabilities are important to model accurately as they are important fluid mixing mechanisms [3] occurring in supernovae and can limit

thermonuclear fuel compression in ICF [4].

In the present study, a multicomponent (two species) Reynolds-averaged Navier–Stokes (RANS) model based on a two-equation K-ϵ turbulence model was used to simulate reshocked Richtmyer–Meshkov instability for shock Mach number $Ma_s = 1.45$ and Atwood number $At = (\rho_{\text{air}} - \rho_{\text{SF}_6})/(\rho_{\text{air}} + \rho_{\text{SF}_6}) = -0.67$. The model equations were solved using a conservative finite-difference weighted nonoscillatory (WENO) shock-capturing method and a characteristic projection formulation. The governing equations account for heat conduction, viscous effects, and enthalpy diffusion, unlike previous studies [5, 6, 10, 11] in which the Reynolds-averaged Euler equations were considered. The present investigation elucidates the sensitivity of the predicted mixing layer widths before and after reshock to variations in the key model coefficients and initial conditions for the heavy-to-light gas transition case.

This paper is organized as follows. Previous modeling of Richtmyer–Meshkov instability corresponding to $At = 0.67$ for three shock Mach numbers using the present model is summarized in Sec. 2. The Richtmyer–Meshkov instability experiment modeled in the current study is briefly summarized in Sec. 3. Governing equations for the multicomponent RANS model used in the simulations, model initial conditions, and numerical method are discussed in Sec. 4. Numerical results for the mixing layer evolution obtained by varying the principal model coefficients and initial conditions are presented and discussed in Sec. 5. Finally, the conclusions of this study are given in Sec. 6.

2 Summary of Previous Modeling of Reshocked Richtmyer–Meshkov Instability Corresponding to the Light-to-Heavy Transition

Modeling turbulent mixing generated via reshocked Richtmyer–Meshkov instability is a topic of current interest. Depending on the turbulence model and numerical approach used to simulate this instability, a variety of issues need be considered. For example, the results are sensitive to initial conditions and key model coefficients, and to variations in these quantities.

To better understand the physical mechanisms by which reshocked Richtmyer–Meshkov instability generates turbulent mixing, Morán-López and Schilling [16] modeled three Richtmyer–Meshkov instability shock tube experiments performed by Vetter and Sturtevant [7] with Atwood number $At = 0.67$. A shock was generated in air a distance $\delta = 2.00$ cm from the air/SF_6 interface, impulsively accelerating the lighter gas towards the heavier gas. The shock Mach numbers were $Ma_s = 1.24$, 1.50, and 1.98 with corresponding test sections and total measurement times $\delta = 110$ cm with $\tau \approx 17$ ms, $\delta = 61$ cm with $\tau \approx 6.0$ ms, and $\delta = 49$ cm with $\tau \approx 2.3$ ms, respectively. Mixing layer widths were compared with the experimental data of Vetter and Sturtevant [7], three-equation BHR model predictions [6], and the power-law self-similar solution prior to reshock.

In varying the initial turbulent kinetic energy seed, K_0, it was found that changes in K_0 had a more significant effect on the predicted mixing layer width *before reshock*, while the width after reshock remained relatively unchanged. Conversely, decreasing the key model coefficients σ_ρ and $C_{\epsilon 0}$ in the shock production terms in the K and ϵ equations increased the turbulent mixing *after reshock*, while having minimal effect on the initial growth. Similarly, increasing the shock Mach number steepened the mixing layer widths and led to an increase in the post-reshock widths. Although the growth prior to reshock was relatively unaffected with changes in Ma_s, reshock occurred earlier in time. Therefore, decreasing σ_ρ and $C_{\epsilon 0}$ and increasing Ma_s resulted in an increase in mixing due to turbulence. Shock production (pressure work), shear production, turbulent dissipation, and turbulent diffusion mechanisms were also considered by examining the budgets in the turbulent kinetic energy equation. The further theoretical development and assessment of turbulence models [5, 6] validated against experimental data [7, 9] predicting reshocked mixing layer growth are important areas of contemporary hydrodynamic instability research. The present investigation considers similar studies for a reversed order of gases, i.e., $At = -0.67$, in which the shock is generated in the heavy gas (SF_6) and accelerated towards the light gas (air).

3 Description of reshocked Richtmyer–Meshkov instability experiment for $Ma_s = 1.45$ and $At = -0.67$

One subset of Richtmyer–Meshkov instability experimental data used to validate the present K-ϵ model was generated by Poggi, Thorembey, and Rodriguez [9]. Air and sulfur hexafluoride (SF_6) were the light and heavy gases, respectively, and the prescribed shock Mach number was $Ma_s = 1.45$. In this experiment the heavy gas was accelerated towards the lighter gas by an upward propagating shock wave in a vertical shock tube. The Atwood number and air test section length for this experiment were $At = -0.67$ and $\delta = 30$ cm, respectively. Schlieren visualization was performed to measure the time-dependent location and thickness of the mixing layer; the two gases were separated by placing a thin wire mesh directly above a plastic membrane 0.30 μm thick.

4 Reynolds-Averaged Navier–Stokes Model and Numerical Method

4.1 Governing Equations and Model Description

The closed single-velocity, multicomponent Reynolds-averaged Navier–Stokes equations describing the transport of mass, momentum, total energy, and heavy gas mass fraction are

$$\frac{\partial \overline{\rho}}{\partial t} + \frac{\partial}{\partial x_j}(\overline{\rho}\,\widetilde{v}_j) = 0\,, \tag{1}$$

$$\frac{\partial}{\partial t}(\overline{\rho}\,\widetilde{v}_i) + \frac{\partial}{\partial x_j}(\overline{\rho}\,\widetilde{v}_i\,\widetilde{v}_j) = -\frac{\partial \overline{p}}{\partial x_i} - \frac{\partial \tau_{ij}}{\partial x_j} + \frac{\partial\,\overline{\sigma}_{ij}}{\partial x_j}\,, \tag{2}$$

$$\begin{aligned}\frac{\partial}{\partial t}(\overline{\rho}\,\widetilde{e}) + \frac{\partial}{\partial x_j}(\overline{\rho}\,\widetilde{e}\,\widetilde{v}_j) \;=\; & -\frac{\partial}{\partial x_j}\left(\frac{\overline{p}\,\nu_t}{\sigma_\rho\,\overline{\rho}}\,\frac{\partial \overline{\rho}}{\partial x_j}\right) - \frac{\partial}{\partial x_j}(\overline{p}\,\widetilde{v}_j) - \frac{\partial}{\partial x_j}(\tau_{ij}\,\widetilde{v}_i) \\ & + \frac{\partial}{\partial x_j}\left(\overline{\kappa}\,\frac{\partial \widetilde{T}}{\partial x_j} + \frac{\mu_t}{\sigma_U}\,\frac{\partial \widetilde{U}}{\partial x_j}\right) + \frac{\partial}{\partial x_j}\left[\left(\overline{\mu} + \frac{\mu_t}{\sigma_K}\right)\frac{\partial K}{\partial x_j}\right] + \frac{\partial \overline{H}_j}{\partial x_j}\,,\end{aligned} \tag{3}$$

$$\frac{\partial}{\partial t}(\overline{\rho}\,\widetilde{m}_H) + \frac{\partial}{\partial x_j}(\overline{\rho}\,\widetilde{m}_H\,\widetilde{v}_j) = \frac{\partial}{\partial x_j}\left(\overline{\rho}\,\overline{D}\frac{\partial \widetilde{m}_H}{\partial x_j}\right) + \frac{\partial}{\partial x_j}\left(\frac{\mu_t}{\sigma_m}\,\frac{\partial \widetilde{m}_H}{\partial x_j}\right), \tag{4}$$

respectively. The quantities $\overline{\rho}$, $\widetilde{v}_i$, $\widetilde{m}_H$, and $\widetilde{e} = \widetilde{v}^2/2 + \widetilde{U} + K$ denote the mean density, velocity, heavy mass fraction, and total energy, respectively; K is the turbulent kinetic energy and $\widetilde{m}_L = 1 - \widetilde{m}_H$ is the light mass fraction (the subscripts H and L denote heavy and light). The dimensionless model coefficients appearing in these equations are σ_ρ, σ_U, σ_K, and σ_m. The gases are assumed to satisfy the ideal gas equation of state, where the mean internal energy and mixture ratio of specific heats are

$$\widetilde{U} = \frac{\overline{p}}{(\overline{\gamma} - 1)\,\overline{\rho}} = c_v\,\widetilde{T}\;\;, \quad \overline{\gamma} = \frac{c_p}{c_v} = \frac{c_{pH}\,\widetilde{m}_H + c_{pL}\,(1 - \widetilde{m}_H)}{c_{vH}\,\widetilde{m}_H + c_{vL}\,(1 - \widetilde{m}_H)}\,, \tag{5}$$

respectively; $c_{pH,L}$ and $c_{vH,L}$ are the specific heats at constant pressure and volume (each assumed to be constant for each gas).

Binary mixture relations [8]

$$\overline{\phi} = \frac{\phi_H\,\widetilde{m}_H/\sqrt{MW_H} + \phi_L\,(1 - \widetilde{m}_H)\,/\sqrt{MW_L}}{\widetilde{m}_H/\sqrt{MW_H} + (1 - \widetilde{m}_H)\,/\sqrt{MW_L}} \tag{6}$$

are used for the molecular transport coefficients, where $\phi = \mu$, D, and κ are the dynamic viscosity, mass diffusivity, and thermal conductivity, respectively (each assumed to be constant for each gas). The heavy and light gas molecular weights are $MW_{H,L}$. The mean enthalpy diffusion term in Eq. (3) is $\overline{H}_j = -\sum_{r=1}^{2} \widetilde{h}_r \overline{J}_{r,j}$, where $\widetilde{h}_r = \widetilde{U}_r + \overline{p}_r/\overline{\rho}_r$ is the mean enthalpy of gas r and $\overline{J}_{r,j} = -\overline{\rho}\left(D_r \partial \widetilde{m}_r/\partial x_j - \widetilde{m}_r \sum_{s=1}^{2} D_s \partial \widetilde{m}_s/\partial x_j\right)$

is the diffusive flux of gas r; the indices 1 and 2 refer to H and L, respectively.

Defining the turbulent kinetic energy dissipation rate, ϵ, and dimensionless model coefficient $C_\mu = 0.09$, the turbulent viscosity is

$$\nu_t = \frac{\mu_t}{\overline{\rho}} = \frac{C_\mu K^2}{\epsilon}\,. \tag{7}$$

The classical Boussinesq Reynolds stress tensor is

$$\tau_{ij} = \frac{2}{3}\,\overline{\rho}\,K\,\delta_{ij} - 2\,\mu_t\left(\widetilde{S}_{ij} - \delta_{ij}\,\frac{\widetilde{S}_k^{\,k}}{3}\right), \tag{8}$$

where $\widetilde{S}_{ij} = (1/2)(\partial\widetilde{v}_i/\partial x_j + \partial\widetilde{v}_j/\partial v_i)$ is the mean strain-rate tensor. The mean viscous stress tensor is

$$\overline{\sigma}_{ij} = \overline{\mu}\left(\frac{\partial\widetilde{v}_i}{\partial x_j} + \frac{\partial\widetilde{v}_j}{\partial x_i} - \frac{2}{3}\,\delta_{ij}\,\frac{\partial\widetilde{v}_k}{\partial x_k}\right) \tag{9}$$

with bulk viscosity neglected.

The closed turbulent kinetic energy and turbulent kinetic energy dissipation rate equations are [10, 16]

$$\frac{\partial}{\partial t}(\overline{\rho}\,K) + \frac{\partial}{\partial x_j}(\overline{\rho}\,K\,\widetilde{v}_j) = -\frac{\nu_t}{\sigma_\rho\,\overline{\rho}}\,\frac{\partial\overline{\rho}}{\partial x_j}\,\frac{\partial\overline{p}}{\partial x_j} - \tau_{ij}\frac{\partial\widetilde{v}_i}{\partial x_j} - \overline{\rho}\,\epsilon + \Pi_K + \frac{\partial}{\partial x_j}\left[\left(\overline{\mu} + \frac{\mu_t}{\sigma_K}\right)\frac{\partial K}{\partial x_j}\right], \tag{10}$$

$$\begin{aligned}\frac{\partial}{\partial t}(\overline{\rho}\,\epsilon) + \frac{\partial}{\partial x_j}(\overline{\rho}\,\epsilon\,\widetilde{v}_j) \;=\; & -C_{\epsilon 0}\,\frac{\epsilon}{K}\,\frac{\nu_t}{\sigma_\rho\,\overline{\rho}}\,\frac{\partial\overline{\rho}}{\partial x_j}\,\frac{\partial\overline{p}}{\partial x_j} - C_{\epsilon 1}\,\frac{\epsilon}{K}\tau_{ij}^d\frac{\partial\widetilde{v}_i}{\partial x_j} - \frac{2}{3}\,C_{\epsilon 3}\,\overline{\rho}\,\epsilon\frac{\partial\widetilde{v}_j}{\partial x_j} - C_{\epsilon 2}\,\frac{\overline{\rho}\,\epsilon^2}{K} \\ & + C_{\epsilon 4}\,\frac{\epsilon}{K}\Pi_K + \frac{\partial}{\partial x_j}\left[\left(\overline{\mu} + \frac{\mu_t}{\sigma_\epsilon}\right)\frac{\partial\epsilon}{\partial x_j}\right],\end{aligned} \tag{11}$$

respectively, where $\tau_{ij}^d = -2\mu_t\left(\widetilde{S}_{ij} - \delta_{ij}\widetilde{S}_k^{\,k}/3\right)$ is the deviatoric part of the Reynolds stress tensor and σ_ϵ, $C_{\epsilon 0}$, $C_{\epsilon 1}$, $C_{\epsilon 2}$, $C_{\epsilon 3}$, and $C_{\epsilon 4}$ are dimensionless model coefficients. The pressure–dilatation correlation, $\Pi_K = \overline{p'\partial v_j''/\partial x_j}$, is not currently included in the simulations.

4.2 Initial conditions, key model coefficients, and self-similarity

The turbulent kinetic energy and turbulent kinetic energy dissipation rate are initialized as constants throughout the domain as

$$K(x,0) = K_0\,(At\,v_1)^2 \quad , \quad \epsilon(x,0) = K(x,0)\,\omega\,, \tag{12}$$

with initial turbulence seed K_0, Atwood number At, post-shock velocity v_1, and linear Richtmyer growth rate $\omega = (2\,\pi/\lambda_{rms})\,|At|\,\Delta v$. The rms wavenumber is $k_{rms} = 2\pi/\lambda_{rms}$, Δv is the change in the interface velocity due to the passage of the shock [12], and $\lambda_{rms} = 0.50$ cm is taken to be an initial rms perturbation wavelength [8]. Thus, the initial turbulent kinetic energy is proportional to v_1^2 and the initial turbulent kinetic energy dissipation rate is related to $K(x,0)$ by the linear growth rate of an rms perturbation, rather than an arbitrary value or a value based on a 'turbulent' lengthscale through the dimensional relation $\epsilon(x,0) = C_\epsilon K(x,0)^{3/2}/L(x,0)$ [where C_ϵ and $L(x,0)$ must be specified].

The model coefficients kept constant throughout the simulations were $C_{\epsilon 1} = 1.44$, $C_{\epsilon 2} = 1.92$, and $C_{\epsilon 3} = 2.00$. Values of $C_{\epsilon 1}$ and $C_{\epsilon 2}$ are standard values for shear turbulence [13], while the value of $C_{\epsilon 3}$ is chosen to be consistent with shockless rapid compression (see [5] for a derivation corresponding to the K-L model). The coefficients varied in the simulations are σ_ρ, $C_{\epsilon 0}$, and $\sigma_m = \sigma_U = \sigma_K = \sigma_\epsilon$, which affect the magnitude of the K and ϵ shock production terms [the first terms on the right sides of Eqs. (10) and (11)].

The analytical late-time self-similar mixing layer width prior to reshock is

$$h(t) = h_0\left(\frac{t}{t_0} + 1\right)^\theta \tag{13}$$

with $t_0 = \theta h_0/\Delta v$ and power-law exponent $\theta = (2C_{\epsilon 2} - 3)/(3C_{\epsilon 2} - 3) \approx 0.30$ (see [5] for a derivation of the self-similar mixing layer width corresponding to the K-L model). Note that self-similarity requires $\sigma_m = \sigma_U = \sigma_K = \sigma_\epsilon$, and these coefficients are chosen here to be smaller than their typical shear flow values close to unity. The expression for $h(t)$ can be derived by solving a simplified form of the one-dimensional Reynolds-averaged equations, in which the shock is treated as an impulse, $\widetilde{v}_i = 0$, $\tau_{ij} = 0$, and $\overline{\mu} = 0$. The resulting reduced K and ϵ equations include only the dissipation and turbulent diffusion terms, and can be solved analytically using the self-similar scaling variable $\eta = 2x/h(t)$ with $h(t)$ given by Eq. (13).

4.3 Numerical method

Inviscid (advective) flux reconstruction is achieved using a conservative Eulerian finite-difference weighted essentially nonoscillatory (WENO) shock-capturing method and a characteristic projection formulation [14, 15]. The numerical implementation includes four mean flow equations and four turbulence model equations (two of which correspond to scalar turbulence variables that are not considered in the present study). The 8×8 left and right eigenvector matrices resulting from the Jacobian of the fluxes are used to project the fluxes between characteristic and physical space, together with Lax–Friedrich flux-splitting and Roe averaging generalized to multicomponent flow (*i.e.*, to include the mean mass fraction equation and a variable $\overline{\gamma}$) and to additional turbulent transport equations. An explicit third-order TVD Runge–Kutta method is used for the time-evolution (a CFL number of 0.2 was used for all simulations); all first and second spatial derivatives are calculated using centered WENO derivatives.

The present investigation considers (formally) third-order reconstruction. As shown in Sec. 5, good agreement is obtained with experimental data and with the analytical self-similar solution prior to reshock. No shock-detection is used to activate the turbulent production terms [the first terms on the right sides of Eqs. (10) and (11)] when a shock is present locally. The velocity satisfied a reflecting boundary condition at the endwall of the test section, and the computational domain was chosen large enough to allow the mixing layers to evolve without waves traveling back from the left boundary and interacting with the interface. The computational grid was uniformly spaced in x, and 9600 grid points were used in each simulation.

5 Numerical Results

A quantity measured in numerical simulations and experiments when studying turbulent mixing induced by hydrodynamic instabilities is the total mixing layer width as a function of time t,

$$h(t) = h_s(t) - h_b(t)\,, \tag{14}$$

which is the difference between the spike and bubble locations, $h_s(t)$ and $h_b(t)$, respectively. During the mixing of gases with different densities, 'spikes' of heavier gas interpenetrate into 'bubbles' of lighter gas. Using the heavy gas mole fraction

$$\widetilde{X}_H = \frac{\widetilde{m}_H\, MW_L}{(MW_L - MW_H)\,\widetilde{m}_H + MW_H}\,, \tag{15}$$

the bubble and spike locations are determined by $h_b(t) = \widetilde{X}_H \leq 1 - \eta$ and $h_s(t) = \widetilde{X}_H \geq \eta$. The mole fraction limit for this study is $\eta = 0.02$, although values $\eta = 0.01$ and 0.05 are often also used. Criteria based on the mass fraction or volume fraction are other options for computing the the spike and bubble locations.

A computational domain of length $X = 70$ cm with a 30 cm test section was used when performing the $Ma_s = 1.45$ Richtmyer–Meshkov instability study. In the present investigation the shock was generated in SF_6 a distance $\delta_s = 0.13$ cm from the SF_6/air interface, with shock and interface locations at $x = 39.87$ cm and $x = 40$ cm, respectively. In a previous study [16], a distance $\delta = 2$ cm between shock and interface was used. However, it was found that a shorter distance was necessary here, as too much turbulent kinetic energy was dissipated before the shock interacted with interface, resulting in smaller mixing layer widths after reshock.

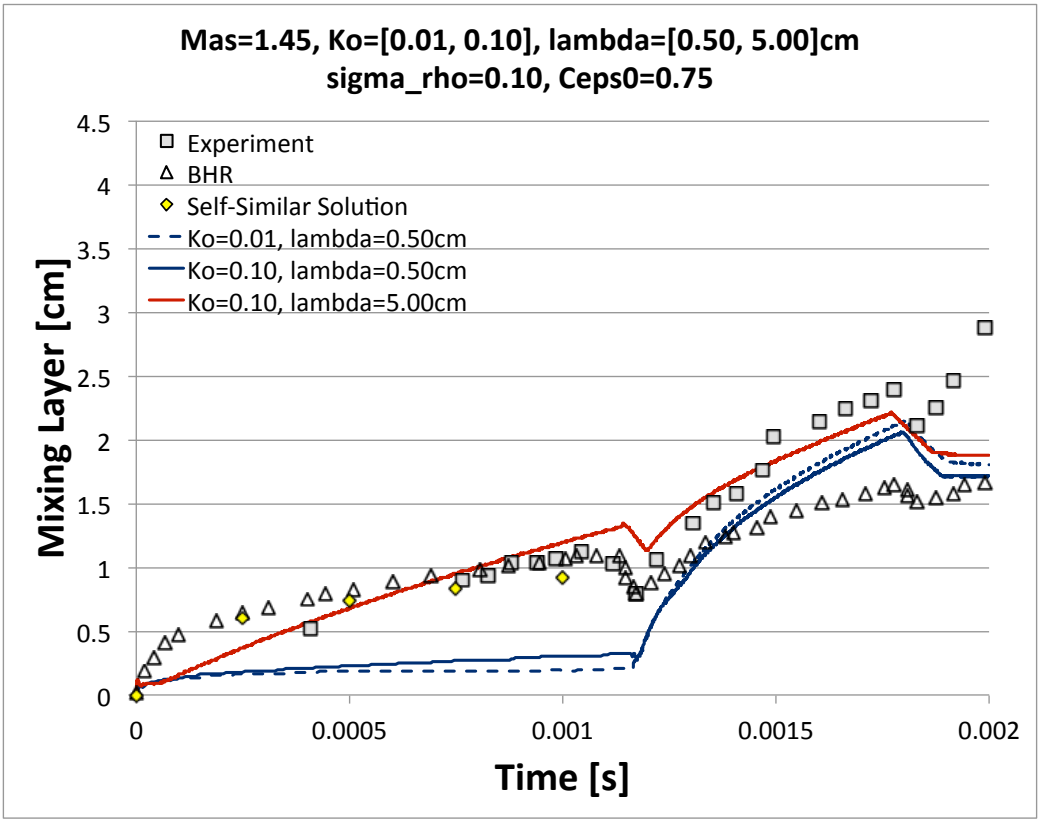

Figure 1: $Ma_s = 1.45$ predicted mixing layer widths for $K_0 = 10^{-1}$, 10^{-2}, $\lambda_{rms} = 0.50$, 5.00 cm, $\sigma_\rho = 0.10$, $\sigma_m = \sigma_U = \sigma_K = \sigma_\epsilon = 0.50$ and $C_{\epsilon 0} = 0.75$. The experimental data points are from Ref. [9], the BHR results are from Ref. [6], and the self-similar solution is given by Eq. (13).

5.1 Sensitivity to variations in initial conditions and Mach number

Figure 1 shows mixing layer widths $h(t)$ obtained by varying the turbulent kinetic energy seed $K_0 = 10^{-1}$, 10^{-2} and initial rms perturbation wavelength $\lambda_{rms} = 0.50$, 5.00 cm with shock production coefficients $\sigma_\rho = 0.10$ and $C_{\epsilon 0} = 0.75$, and diffusion coefficients $\sigma_m = \sigma_U = \sigma_K = \sigma_\epsilon = 0.50$. The computed mixing layer is compared with experimental data from Poggi, Thorembey, and Rodriguez [9], BHR model predictions [6], and the self-similar solution Eq. (13) prior to reshock.

Previous Richtmyer–Meshkov instability modeling with $At = 0.67$ [16] demonstrated that $K_0 = 10^{-1}$ and 10^{-2} and $\lambda_{rms} = 0.50$ cm yielded results in good agreement with the experimental mixing layer width prior to reshock for shock Mach numbers $Ma_s = 1.24$, 1.50, and 1.98. However, in reversing the order of the gases ($At = -0.67$) the same initial conditions underpredict the initial width by approximately 0.75 cm at the location of largest disagreement (see Fig. 1). Typically, the initial turbulent kinetic energy seed is a fraction of the postshock velocity squared and is not increased past a value $K_0 = 10^{-1}$. Therefore, λ_{rms} was increased to dissipate less turbulent kinetic energy at the initial time. Increasing the initial rms perturbation wavelength to $\lambda_{rms} = 5.00$ cm resulted in changes throughout the mixing layer width, but with a more significant increase prior to reshock.

Prior to reshock, the width increases nearly linearly and deviates from the self-similar solution before $t \approx 0.5$ ms and matches it more closely afterwards. However, despite the deviation at early times, the predicted width agrees with the experimental data more closely. After reshock, the mixing layer width also increases from that generated with the original initial conditions while maintaining the same profile, unlike prior to reshock. Similar to the BHR model, the width deviates from the additional turbulent mixing apparent at $t \approx 1.88$ ms where a second shock interacts with the layer, leading to additional turbulent mixing. Such additional mixing at later times is independent of the initial conditions, and therefore modifications in

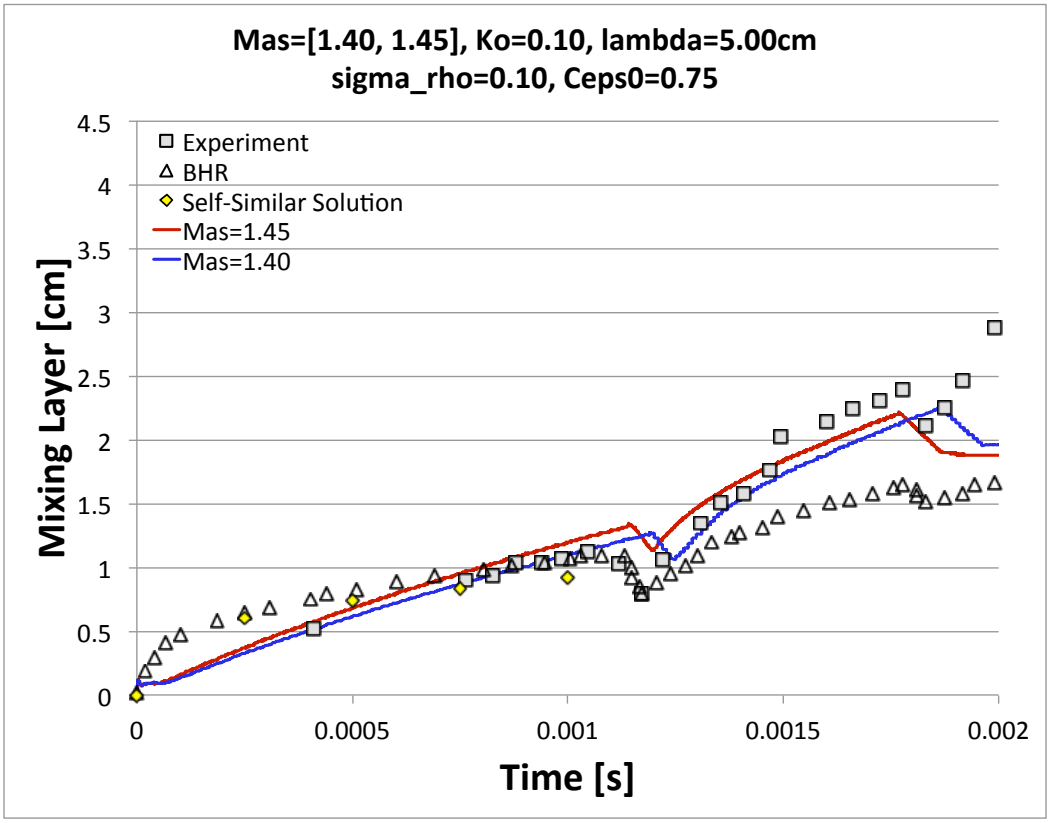

Figure 2: Predicted mixing layer widths for $Ma_s = 1.45$ and 1.40; $K_0 = 10^{-1}$, $\lambda_{rms} = 5.00$ cm, $\sigma_\rho = 0.10$, $\sigma_m = \sigma_U = \sigma_K = \sigma_\epsilon = 0.50$ and $C_{\epsilon 0} = 0.75$. The experimental data points are from Ref. [9], the BHR results are from Ref. [6], and the self-similar solution is given by Eq. (13).

key model coefficients may be necessary to better match the experiment at later times.

Figure 2 shows the sensitivity of the predicted mixing layer widths to variations in incident shock Mach number. Variations in Ma_s were also considered in the light-to-heavy case [16]. Using $Ma_s = 1.45$ as a reference value, a lower incident shock Mach number $Ma_s = 1.40$ was also considered in the present study. Changes in the predicted mixing layer width were noted before and after reshock when comparing the $Ma_s = 1.40$ and $Ma_s = 1.45$ results. The initial width for $Ma_s = 1.40$ was lower but remained close to the experimental data. Also, reshock occurred at a later time $\tau_r \approx 1.22$ ms as expected, because the shock travels at a lower speed at smaller Ma_s. The predicted mixing layer width was also lower for $Ma_s = 1.40$ after reshock. Similar results were seen in [16], where the mixing layer after reshock increased in magnitude with larger incident Mach numbers. This is additional evidence that the turbulent kinetic energy available for turbulent mixing increases correspondingly with Ma_s. As with variations in K_0 and λ_{rms}, variations in Ma_s do not have an effect on the additional mixing apparent at $t \approx 1.88$ ms due to the second reshock, additionally indicating that changes in key model coefficients may be required to better predict the experimental data.

5.2 Variations in model coefficients $C_{\epsilon 0}$ and σ_ρ

From Sec. 5.1 $K_0 = 10^{-1}$, $\lambda_{rms} = 5.00$ cm, $C_{\epsilon 0} = 0.75$, $\sigma_\rho = 0.10$, and $\sigma_m = \sigma_U = \sigma_K = \sigma_\epsilon = 0.50$ are an initial condition and coefficient set that yields numerical results in good agreement with the experimental data. Using these values, additional model sensitivity studies to changes in the shock production model coefficients $C_{\epsilon 0}$ and σ_ρ were performed.

Figure 3 illustrates the sensitivity to changes in the dissipation rate shock production model coefficient $C_{\epsilon 0}$, in conjunction with changes in the incident shock Mach number. Selecting a reference value $C_{\epsilon 0} = 0.75$, simulations were performed with a variation in this coefficient. Simulations were also performed for a smaller

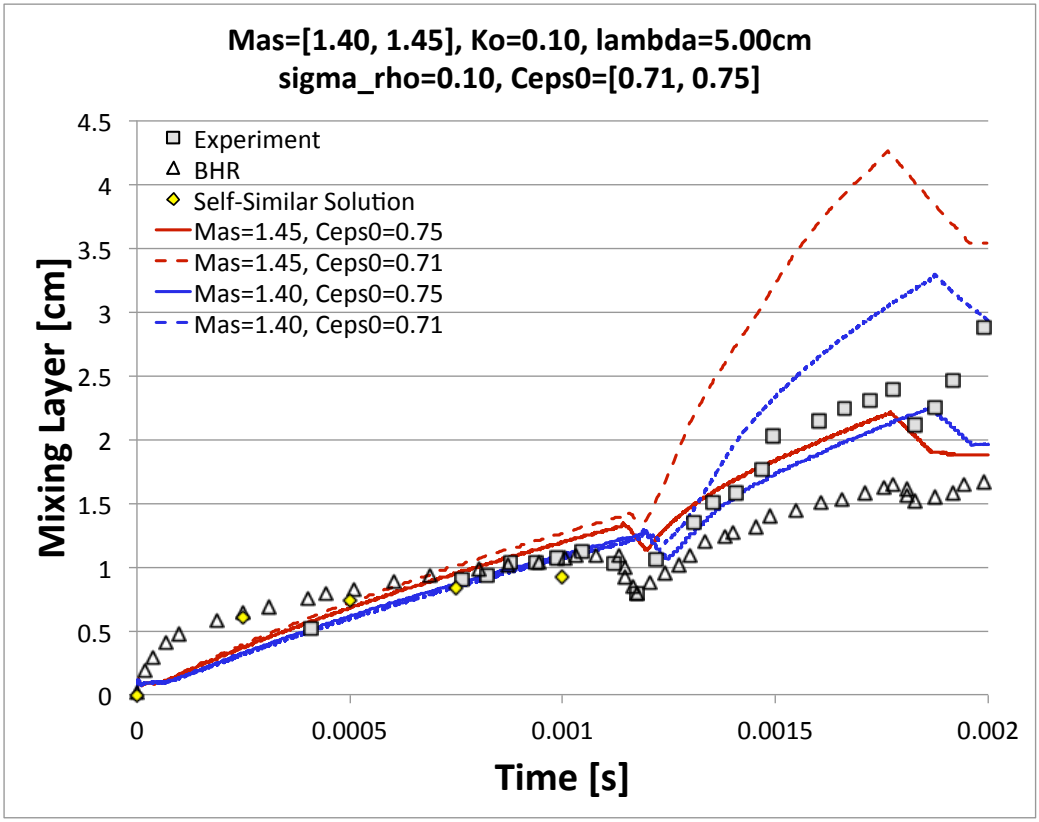

Figure 3: Predicted mixing layer widths for $Ma_s = 1.45$ and 1.40, $K_0 = 10^{-1}$, $\lambda_{rms} = 5.00$ cm, $\sigma_\rho = 0.10$, $\sigma_m = \sigma_U = \sigma_K = \sigma_\epsilon = 0.50$ and $C_{\epsilon 0} = 0.75$ and 0.71. The experimental data points are from Ref. [9], the BHR results are from Ref. [6], and the self-similar solution is given by Eq. (13).

$C_{\epsilon 0}$ value: decreasing the value from 0.75 to 0.71 did not strongly affect the mixing layer width prior to reshock, but a significant increase was seen in the post-reshock width. An increase in mixing is expected as smaller values of $C_{\epsilon 0}$ decrease the amount of turbulent kinetic energy dissipation production in the flow, resulting in an increase of turbulent mixing; similar results were observed elsewhere [16]. Figure 3 demonstrates that this small decrease in $C_{\epsilon 0}$ resulted in a 2.0 cm increase in the width at the time of most mixing, $t \approx 1.88$ ms. Also presented in Fig. 3 are corresponding results for variation in shock Mach number $Ma_s = 1.40$: similar behavior is observed as with $Ma_s = 1.45$. The mixing layer increases significantly after reshock while the initial width remains relatively unaffected. The mixing layer width is approximately 1.0 cm lower for $Ma_s = 1.40$ than for $Ma_s = 1.45$.

The other model coefficient considered was σ_ρ, which appears inversely in both the turbulent kinetic energy and dissipation rate shock production terms. Increasing σ_ρ decreases the amount of turbulence generation via shock production, which has an important role in post-reshock turbulent mixing and has a small influence on the initial width. As illustrated in Fig. 4 where results are compared using $\sigma_\rho = 0.10$ and 0.20, the results are very sensitive to changes in σ_ρ. Similar effects were reported in [16], but the effect is more pronounced in the present study where $At = -0.67$. Simulations were also performed using the same values for $C_{\epsilon 0}$ as in Fig. 3 to further explore the mixing layer sensitivity to changes in σ_ρ when also varying $C_{\epsilon 0}$. In varying these coefficients, it is evident that using $\sigma_\rho = 0.20$ significantly underpredicts the mixing layer width following reshock, almost eliminating any further turbulent layer growth. Although $C_{\epsilon 0}$ variations can affect the width following reshock, σ_ρ appears to be the dominant coefficient as the width assumes the same values after reshock for $\sigma_\rho = 0.20$ for all values of $C_{\epsilon 0}$. It is not until $t \approx 1.88$ ms that effects due to variations in $C_{\epsilon 0}$ become evident. Finally, Fig. 4 also shows that unlike changes in $C_{\epsilon 0}$, variations in σ_ρ produced changes in the initial width. Thus, augmenting the value of σ_ρ increased the predicted mixing layer width prior to reshock and reduced the amount of turbulent mixing following reshock.

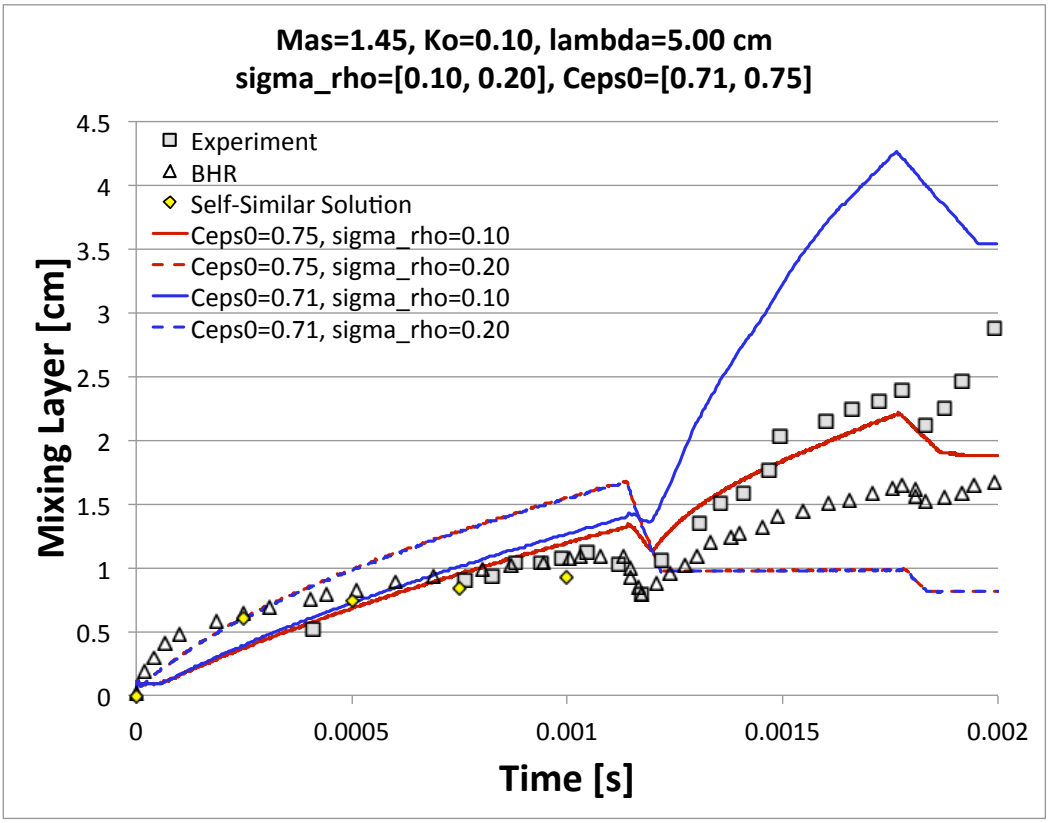

Figure 4: Predicted mixing layer widths for $Ma_s = 1.45$, $K_0 = 10^{-1}$, $\lambda_{rms} = 5.00$ cm, $\sigma_\rho = 0.10$ and 0.20, $\sigma_m = \sigma_U = \sigma_K = \sigma_\epsilon = 0.50$ and $C_{\epsilon 0} = 0.75$ and 0.71. The experimental data points are from Ref. [9], the BHR results are from Ref. [6], and the self-similar solution is given by Eq. (13).

6 Conclusions

The present study used a multicomponent (two species) Reynolds-averaged Navier–Stokes (RANS) two-equation K-ϵ turbulence model to simulate reshocked Richtmyer–Meshkov instability for shock Mach number $Ma_s = 1.45$ and Atwood number $At = -0.67$. Mixing layer widths were compared with SF_6/air experimental data from Poggi, Thorembey, and Rodriguez [9]. Additional comparisons were made with numerical results from the three-equation BHR turbulence model for $Ma_s = 1.45$ [6] and the power-law self-similar solution prior to reshock.

The first set of simulations considered the sensitivity of the predicted mixing layer width to variations in initial conditions including the turbulent kinetic energy seed K_0, initial rms perturbation wavelength λ_{rms}, and incident shock Mach number $Ma_s = 1.45$. Using $K_0 = 0.10$ and 0.01 with $\lambda_{rms} = 0.50$ cm underpredicted the experimental data throughout. However, using $\lambda_{rms} = 5.00$ cm produced better results. Furthermore, although $\lambda_{rms} = 5.00$ cm caused the predicted mixing layer width to deviate from the self-similar solution at early times, it agreed with the experimental data very well. Variations in the incident shock Mach number had a more significant effect after reshock. *Prior* to reshock, smaller values in Ma_s resulted in a decrease in initial growth and later reshock times.

The second set of investigations considered variations in shock production model coefficients $\sigma_\rho = 0.10$, 0.20 and $C_{\epsilon 0} = 0.75$, 0.71 also in conjunction with incident shock Mach number variations $Ma_s = 1.45$ and 1.40. For both incident shock Mach numbers $Ma_s = 1.45$ and 1.40, a decrease in $C_{\epsilon 0}$ from 0.75 to 0.71 led to an increase in the post-reshock width. Increasing σ_ρ from 0.10 to 0.20 significantly decreased the amount of turbulent mixing after reshock, nearly suppressing any further mixing. Thus, σ_ρ was the dominant model coefficient in determining the amount of turbulent kinetic energy available for mixing after reshock, with $\sigma_\rho = 0.10$ producing results in best overall agreement with the experimental data.

Grid refinement studies are planned to assess convergence of the mixing layer width and other quantities. Additional studies are also planned to consider the budgets of the turbulent kinetic energy and dissipation rate equations to further understand the generation and evolution of turbulent mixing induced by reshocked Richtmyer–Meshkov instability. Comparison of the present results to those using fifth-order WENO reconstruction will also be performed. The role of molecular transport processes is also under consideration.

This work was funded by the U. S. Department of Energy NNSA under the Predictive Science Academic Alliances Program by grant DE-FC52-08NA28616 and performed under the auspices of the DOE by Lawrence Livermore National Laboratory under Contract DE-AC52-07NA27344.

References

[1] Y. Zhou, B.A. Remington, H.F. Robey, A.W. Cook, S.G. Glendinning, A. Dimits, A.C. Buckingham, G.B. Zimmerman, E.W. Burke, T.A. Peyser, W. Cabot, D. Eliason, Progress in understanding turbulent mixing induced by Rayleigh–Taylor and Richtmyer–Meshkov instabilities, Phys. Plasmas 10 (2002), 1883–1886.

[2] J. Grun, J. Stamper, C. Manka, J. Resnick, R. Burris, J. Crawford, B.H. Ripin, Instability of Taylor–Sedov blast waves propagating through a uniform gas, Phys. Rev. Lett. 66 (1991), 2738–2741.

[3] B.D. Collins, J.W. Jacobs, PLIF flow visualization and measurements of the Richtmyer–Meshkov instability of an air/SF_6 interface, J. Fluid Mech. 464 (2002), 113–136.

[4] S. Atzeni, J. Meyer-ter-Vehn, *The Physics of Inertial Fusion: Beam Plasma Interaction, Hydrodynamics, Hot Dense Matter*, International Series of Monographs on Physics Vol. 125, Oxford University Press (2004).

[5] G. Dimonte, R. Tipton, *K-L* turbulence model for the self–similar growth of Rayleigh-Taylor and Richtmyer-Meshkov instabilities, Phys. Fluids 18 (2006), 085101.

[6] A. Banerjee, R.A. Gore, M.J. Andrews, Development and validation of a turbulent-mix model for variable density and compressible flows, Phys. Rev. E 82 (2010) 046309.

[7] M. Vetter, B. Sturtevant, Experiments on the Richtmyer-Meshkov instability of an air/SF_6 interface, Shock Waves 4 (1995), 247–252.

[8] D.J. Hill, C. Pantano, D.I. Pullin, Large-eddy simulation and multiscale modeling of a Richtmyer–Meshkov instability with reshock, J. Fluid Mech. 557 (2006), 29–61.

[9] F. Poggi, M.H. Thorembey, G. Rodriguez, Velocity measurements in turbulent gaseous mixtures induced by Richtmyer-Meshkov instability, Phys. Fluids 10 (1998), 2698–2700.

[10] S. Gauthier, M. Bonnet, A k-ϵ model for turbulent mixing in shock-tube flows induced by Rayleigh–Taylor instability, Phys. Fluids A 2 (1990), 1685–1694.

[11] V.P. Chiravalle, The k-L turbulence model for describing buoyancy-driven fluid instabilities, Laser and Particle Beams 24 (2006), 381–394.

[12] O. Schilling, M. Latini, High-order WENO simulations of three-dimensional reshocked Richtmyer–Meshkov instability to late times: Dynamics, dependence on initial conditions, and comparisons to experimental data, Acta Math. Scientia 30 (2010), 595–620.

[13] S.B. Pope, *Turbulent Flows*, Cambridge University Press (2000).

[14] X.-D. Liu, S. Osher, T. Chan, Weighted essentially non-oscillatory schemes, J. Comput. Phys. 115 (1994), 200–212.

[15] C.-W. Shu, High order weighted essentially nonoscillatory schemes for convection dominated problems, SIAM Rev. 51 (2009), 82–126.

[16] J.T. Morán-López, O. Schilling, Multicomponent Reynolds-averaged Navier–Stokes simulations of reshocked Richtmyer–Meshkov instability-induced mixing, High Energy Density Phys. Submitted (2012).

[17] D.C. Wilcox, *Turbulence Modeling for CFD* third edition, DCW Industries, LaCanada, California, (2006) DCW Industries, LaCanada, California (2006).